Fast Control of a Modular Multilevel Converter STATCOM using Optimized Pulse Patterns

Vedrana Spudić, *Member, IEEE* and Tobias Geyer, *Senior Member, IEEE*

***Abstract*—A model predictive control system for delta-connected modular multilevel converter is proposed in this paper. The control system is based on offline computed optimal pulse patterns, which are modified online using model predictive control. Optimized pulse patterns facilitate the shaping of the grid current spectrum at low switching frequencies. Unlike conventional control methods with optimal pulse patterns, the proposed fast control system enables agile dynamic operation beyond nominal conditions. The proposed control system can therefore be applied to STATCOM applications, which require functionalities such as harmonic injection, operation during grid imbalances and fast transients.**

I. Introduction

A static synchronous compensator (STATCOM) is a power converter connected to the electrical grid, whose primary task is to generate or absorb reactive power. Additionally, harmonics and negative-sequence currents resulting from large dynamic loads, such as arc furnaces, can be compensated for. The voltages and currents at the point of common coupling (PCC) with the grid must meet stringent grid codes, which impose limits on the amplitudes of harmonics and inter-harmonics [1].

Modular multilevel converters (MMCs) achieve line-to-line voltages in the medium and high voltage range through the series-connection of unipolar or bipolar modules [2]. This feature makes the MMC topology particularly suited to grid-connected applications like STATCOMs, by reducing or eliminating the coupling transformer [3]. Furthermore, due to the large number of voltage levels that can be generated by an MMC, the grid codes can be met with small or even without output filters.

The MMC requires a sophisticated control and modulation scheme. Ideally, the controller facilitates the reduction of the filter size while meeting the grid codes, and it allows one to operate the converter at low switching frequencies. This minimizes the losses and enables the use of a simpler and cheaper cooling system. Additional requirements are the control of the circulating current in the delta-connected MMC topology, harmonic injection, a fast dynamic behaviour during transients and the ability to operate under unbalanced grid conditions.

A well-known approach for improving the spectral content of the output currents is the use of optimal pulse patterns (OPPs). However, the classical control methodology used with OPP-based modulation, described in e.g. [4] and references thereof, is not suitable for STATCOM applications. More specifically, the application of pre-stored switching angles governed by a slow modulation index selection loop fails to meet the above mentioned control requirements. The literature on OPP-based control methods for STATCOMs is scarce. Reference [5] highlights the benefits of OPPs for MMC, but limits its investigation to steady-state operation.

An OPP-based control system is proposed in this paper, which provides the benefits of OPP-based modulation, while meeting the control objectives that are required for STATCOMs. A fast online controller, called model predictive pulse pattern control (MP^{3}C), directly modifies the OPP switching instants to achieve fast closed-loop current control. The control method described here extends a related methodology applied to medium-voltage drives, see [6] and subsequent work by the authors.

Classical OPP-based control methods require the switching angles to vary smoothly with the modulation index. Such OPPs are suboptimal with regard to their harmonic performance. This is particularly the case for selective harmonic elimination (SHE) patterns, in which a certain number of harmonic amplitudes are set to zero, see e.g. [7]. The smoothness restriction on the switching angles can be dropped for the proposed controller, providing additional degrees of freedom to optimize the harmonic spectrum. In particular, OPPs can be designed such that the harmonic content of the voltages and currents is constrained to the amplitude limits prescribed by the grid codes while minimizing the overall distortions.

This paper focuses on a delta-connected MMC, which is a promising topology for STATCOM applications with the circulating current control being particularly challenging [8]. Nevertheless, the proposed controller can also be applied to other MMC topologies.

II. System Description

The delta-connected MMC STATCOM is connected via the PCC to the grid, as shown in Fig. 1. Other loads connected to the PCC can be considered as a disturbance, which can be modeled as a current source with the three-phase current $i_{\mathrm{l,abc}} = [i_{\mathrm{l,a}}\ i_{\mathrm{l,b}}\ i_{\mathrm{l,c}}]^T$. The grid is modeled with an equivalent Thevenin representation, comprising the sinusoidal three-phase voltage source $v_{\mathrm{abc}} = [v_{\mathrm{a}}\ v_{\mathrm{b}}\ v_{\mathrm{c}}]^T$, the series inductance L_{g} and the grid resistance R_{g}. We also define the three-phase grid current $i_{\mathrm{g,abc}} = [i_{\mathrm{g,a}}\ i_{\mathrm{g,b}}\ i_{\mathrm{g,c}}]^T$.

The delta-connected MMC has three branches. Each branch consists of the series-connection of M bipolar modules, an inductor L_{b} and a (small) resistance R_{b}. The inductance L_{sc}

The authors are with ABB Corporate Research, Baden-Dättwil, Switzerland; e-mail: vedrana.spudic@ch.abb.com, t.geyer@ieee.org

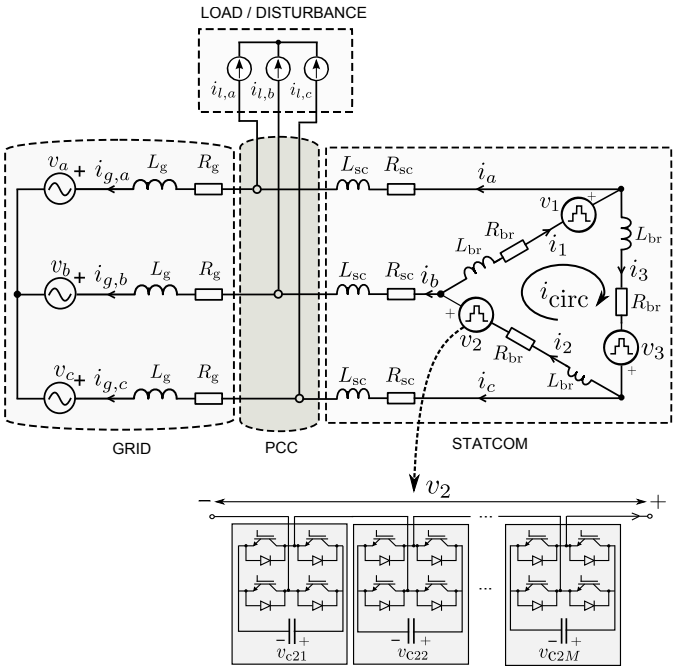

Fig. 1: Delta-connected MMC STATCOM connected to the grid

and resistance R_{sc} model the connection of the MMC to the PCC. This connection typically includes a transformer.

Each module contains two pairs of switches and a capacitor, see Fig. 1. The voltage of the capacitor is denoted by v_{cjk}, where j refers to the branch number and k refers to the module number within that branch. By applying different gate signals to the module's switches, the capacitor is either disconnected from the converter branch or it is connected to the converter branch with a positive or negative polarity. The voltage across the module terminals is $v_{jk} = u_{jk} v_{cjk}$, where $u_{jk} \in \{-1, 0, 1\}$ denotes the switch position, which is the control variable. The voltage of the series-connection of the modules in the jth branch is $v_j = \sum_{k=1}^{M} u_{jk} v_{cjk}$. We refer to v_j, with $j \in \{1, 2, 3\}$, as the branch voltage, and i_j is correspondingly the branch current. We also define the three-phase branch voltage $v_{123} = [v_1 \ v_2 \ v_3]^T$ and branch current $i_{123} = [i_1 \ i_2 \ i_3]^T$.

The circuit in Fig. 1 is described by the following equations that arise from Kirchhoff laws:

$$\begin{aligned} v_{123} &= L_{\text{br}} \frac{di_{123}}{dt} + R_{\text{br}} i_{123} + \\ &+ D_1 \left(v_{\text{abc}} + L_{\text{sc}} \frac{di_{\text{sc,abc}}}{dt} + R_{\text{sc}} i_{\text{abc}} + L_{\text{g}} \frac{di_{\text{g,abc}}}{dt} + R_{\text{g}} i_{\text{g,abc}} \right), \\ i_{\text{abc}} &= D_2 i_{123}, \ i_{\text{g,abc}} = i_{\text{abc}} - i_{\text{l,abc}}, \end{aligned} \tag{1}$$

where $D_1 = \begin{bmatrix} 1 & -1 & 0 \\ 0 & 1 & -1 \\ -1 & 0 & 1 \end{bmatrix}$ and $D_2 = \begin{bmatrix} 1 & 0 & -1 \\ -1 & 1 & 0 \\ 0 & -1 & 1 \end{bmatrix}$.

We multiply (1) with the Clarke transformation matrix

$$M_{\alpha\beta\gamma} = \frac{2}{3} \begin{bmatrix} 1 & -\frac{1}{2} & -\frac{1}{2} \\ 0 & \frac{\sqrt{3}}{2} & -\frac{\sqrt{3}}{2} \\ \frac{1}{2} & \frac{1}{2} & \frac{1}{2} \end{bmatrix}$$

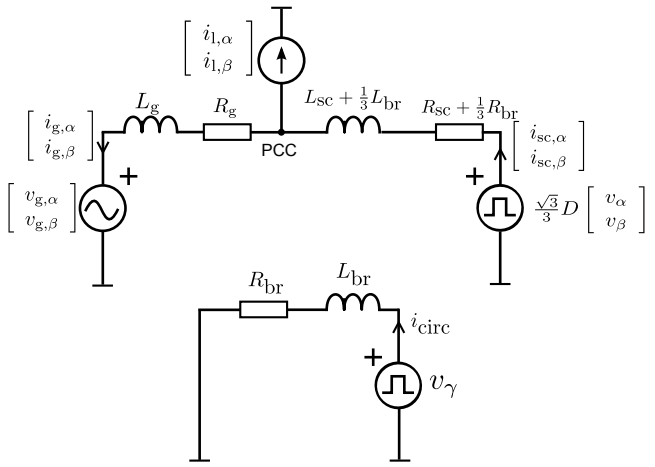

Fig. 2: Equivalent differential-mode and common-mode circuit representations

and introduce the substitutions

$$\begin{aligned} i_{\alpha\beta\gamma} &= M_{\alpha\beta\gamma} i_{abc}, \ v_{\alpha\beta\gamma} = M_{\alpha\beta\gamma} v_{123}, \\ i_{\text{g},\alpha\beta\gamma} &= M_{\alpha\beta\gamma} i_{\text{g},abc}, \ v_{\text{g},\alpha\beta\gamma} = M_{\alpha\beta\gamma} v_{\text{g},abc}. \end{aligned}$$

We then obtain the model

$$\begin{aligned} \frac{\sqrt{3}}{3} D v_{\alpha\beta} &= L_{\text{eq}} \frac{di_{\alpha\beta}}{dt} + R_{\text{eq}} i_{\alpha\beta} + \\ &+ L_{\text{g}} \frac{di_{\text{g},\alpha\beta}}{dt} + R_{\text{g}} i_{\text{g},\alpha\beta} + v_{\text{g},\alpha\beta}, \\ v_\gamma &= L_{\text{br}} \frac{di_{\text{circ}}}{dt} + R_{\text{br}} i_{\text{circ}}, \\ i_{\text{g},\alpha\beta} &= i_{\alpha\beta} - i_{\text{l},\alpha\beta}, \ i_{\text{g},\gamma} = 0, \end{aligned} \tag{2}$$

where $L_{\text{eq}} = L_{\text{sc}} + \frac{1}{3} L_{\text{br}}$ and $R_{\text{eq}} = R_{\text{sc}} + \frac{1}{3} R_{\text{br}}$. The matrix $D = \begin{bmatrix} \frac{\sqrt{3}}{2} & \frac{1}{2} \\ -\frac{1}{2} & \frac{\sqrt{3}}{2} \end{bmatrix}$ performs a clockwise rotation by 30°. This rotation arises from translating the branch quantities from delta to star configuration.

The equations for the differential-mode ($\alpha\beta$) components describe the currents between the grid and the STATCOM. Due to the star connection of the grid, the common-mode grid current component is zero. However, a common-mode component in the branch current does exist. This so-called circulating current $i_{\text{circ}} = \frac{1}{3}(i_1 + i_2 + i_3)$ flows between the converter branches, see Fig. 1. The differential-mode and common-mode circuit diagrams of the delta-connected MMC are depicted in Fig. 2.

III. OPP Computation

OPPs are computed offline such that the desired spectral properties of the STATCOM's output current are achieved. To simplify this procedure, it is common practise to assume operation at steady state and nominal operating conditions, i.e. the module capacitors are assumed to be constant voltage sources v_{c} and disturbances from the grid are neglected. The branch voltages are then given by $v_j = u_j v_{\text{c}}$, $j \in \{1, 2, 3\}$, where $u_j \in \{-M, \ldots, 0, \ldots, M\}$ is a multilevel switching function.

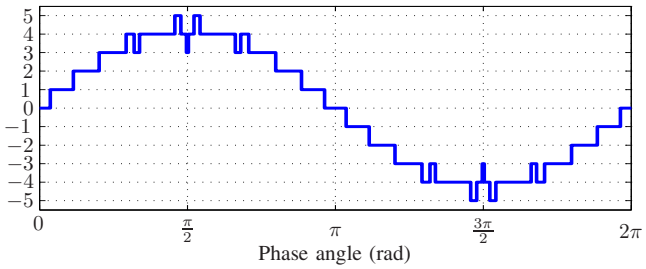

Fig. 3: Quarter-wave symmetric multilevel switching function

We restrict the OPPs to quarter-wave symmetric patterns, for which $u(\pi - \theta) = u(\theta)$ and $u(\theta + \pi) = -u(\theta)$ hold, where θ is the phase angle. Quarter-wave symmetric patterns are, by definition, free of even harmonics. The entire switching pattern can be constructed from the first quarter wave. More specifically, the quarter-wave symmetric pattern is fully described by the primary *switching angles* $\theta_1, \ldots, \theta_d$ at which the switching function changes its value, and the primary sequence of switching transitions (or *switching sequence*) $\Delta u_1, \ldots, \Delta u_d$, with $\Delta u_i \in \{-1, 1\}$. For example, $\Delta u_i = 1$ implies that the value of the switching function increases by 1 at the phase angle θ_i.

The integer d denotes the number of switching events in a quarter-period and is referred to as the *pulse number*. The latter defines the switching frequency of the system. An example of a quarter-wave symmetric multilevel switching function with $d = 9$ is provided in Fig. 3.

Owing to its periodicity and quarter-wave symmetry, the multilevel OPP can be represented by the Fourier series

$$u(\theta) = \sum_{n=1}^{\infty} b_n \sin(n\theta) \tag{3}$$

with the Fourier coefficient

$$b_n = \begin{cases} \frac{4}{n\pi} \sum_{i=1}^{d} \Delta u_i \cos(n\alpha_i), & \text{for odd } n, \\ 0, & \text{for even } n. \end{cases} \tag{4}$$

The design of OPPs is done by solving the following optimization problem for a fixed pulse number d and a fixed fundamental amplitude b_1:

$$\min_{\substack{\theta_1,\ldots,\theta_d \\ \Delta u_1,\ldots,\Delta u_d}} \sum_{\substack{n=2k+1, k\in\mathbb{N} \\ n\leq N}} C_n \left(\frac{1}{n^2} \sum_{i=1}^{d} \Delta u_i \cos(n\theta_i) \right)^2 \tag{5a}$$

$$\text{subj. to } 0 \leq \theta_1 \leq \theta_2 \leq \cdots \leq \theta_d \leq \frac{\pi}{2} \tag{5b}$$

$$\sum_{i=1}^{j} \Delta u_j \leq M, \quad \text{with } 1 \leq j \leq d \tag{5c}$$

$$\frac{4}{\pi} \sum_{i=1}^{d} \Delta u_i \cos(\theta_i) = b_1 \tag{5d}$$

$$\left| \frac{v_\mathrm{c}}{k^2 \omega L_{\mathrm{g,eq}} \pi} \sum_{i=1}^{d} \Delta u_i \cos(k\theta_i) \right| \leq I_{k,\mathrm{lim}}, \forall k \in \mathcal{K}. \tag{5e}$$

The features of this optimization problem are described in the remainder of this section. The switching angles and switching sequence constitute the optimization variables. Since the switching sequence is restricted to the set $\{-1, 0, 1\}$, the optimization problem (5) is a mixed-integer program. Rather than solving the mixed-integer program directly, it can be solved indirectly by enumerating several switching sequences. For a given switching sequence, (5) simplifies to a non-convex but real-valued optimization problem. Such optimization problems can be solved relatively efficiently, but require multiple different initial conditions.

The objective function (5a) penalizes the (weighted) amplitudes of the switching function's harmonic spectrum. Thanks to quarter-wave symmetry, only odd harmonics need to be considered. We distinguish between differential-mode and common-mode harmonics. For a $\frac{2\pi}{3}$ phase shift between the converter branches, all non-triplen harmonics are differential-mode harmonics, which give rise to grid current harmonics. Triplen harmonics constitute common-mode harmonics, which drive circulating current harmonics, see Sect. II. To account for this difference, triplen and non-triplen harmonics can be penalized differently by choosing the weighting coefficients C_n accordingly. If the coefficients for non-triplen harmonics are the same, the objective function penalizes the total harmonic distortion of the output current, see [9]. The highest harmonic order considered in the objective function is denoted by N.

Constraint (5c) in combination with (5b) ensures that the switching pattern can be synthesized by an M-level converter. If enumeration is adopted and the optimization problem is solved for a given switching sequence, which is a-priori feasible, (5c) can be omitted. Constraint (5b) then ensures that the required switching sequence is obtained. Constraint (5d) ensures that the amplitude of the switching function's fundamental component is equal to b_1. The latter influences the fundamental current at the converter output and the power exchange with the grid.

Constraint (5e) ensures that the spectral limits imposed by the grid codes are met. Here v_c denotes again the nominal voltage of the module capacitors, ω is the fundamental frequency and $L_{\mathrm{g,eq}} = L_\mathrm{g} + L_\mathrm{sc} + \frac{1}{3} L_\mathrm{br}$ is the equivalent grid inductance. The relevant grid code defines the limits $I_{k,\mathrm{lim}}$. The set $\mathcal{K}$ contains odd non-triplen harmonic orders, typically up to the harmonic order of 180.

To enable the operation of the system at different operating points (corresponding to e.g. different reactive power references), OPPs are computed for a range of fundamental amplitudes b_1. Moreover, to enable operation at different switching frequencies, the OPPs are typically computed for a range of pulse numbers d. The primary switching angles and primary switching sequences are stored in the controller memory.

IV. OPP-Based MMC Control

The offline computed OPPs are modified online to ensure fast and precise dynamic reference tracking at all operating

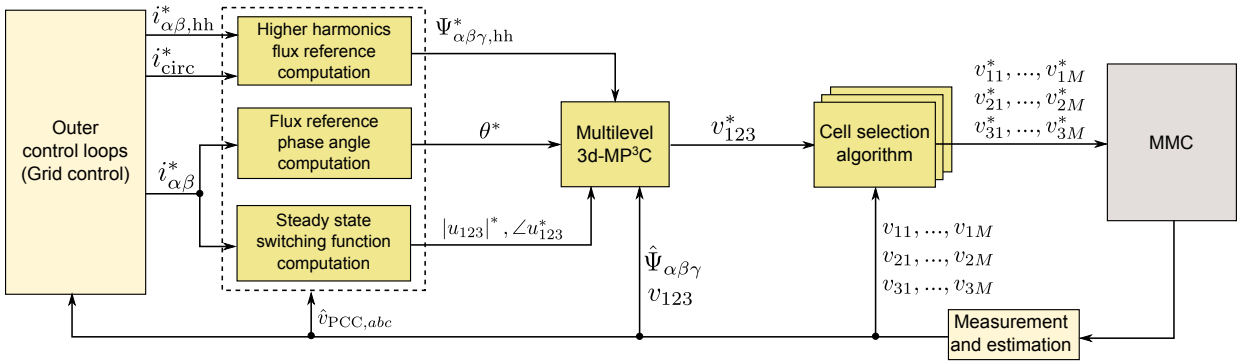

Fig. 4: Block diagram of the OPP-based model predictive control system for the STATCOM

conditions. This is achieved by the proposed control system, whose block diagram is provided in Fig. 4.

A. Outer Control Loops

An upper-level control loop provides the following three references to the inner control loops.

Differential-mode current reference $i^*_{\alpha\beta}$. This reference is typically obtained from the reactive power setpoint Q^* or from the grid voltage regulation loop. During steady-state operation, this reference contains only the fundamental component without additional harmonics.

Higher-order harmonic current reference i^*_{hh}. This reference facilitates the compensation of grid or load harmonic components, which are injected, for example, by arc furnaces. The reference contains the time-evolution of higher-order harmonic currents; it is effectively free of a fundamental component.

Circulating current reference i^*_{circ}. For symmetrical grid conditions, the circulating current reference is typically zero to avoid unnecessary switching and conduction losses. Additional harmonics might be added to the circulating current reference to achieve additional objectives, such as the minimization of the capacitor voltage ripple [10].

B. Virtual Flux Vector and Modeling

The proposed controller regulates virtual flux vectors along their given trajectories. The virtual flux

$$\Psi(t) = \int_{-\infty}^{t} v(\tau)\mathrm{d}\tau, \tag{6}$$

is defined as the time integral of the voltage v. The notion of virtual fluxes generalizes flux linkages in electrical machines. In this paper, we use the terms flux and virtual flux interchangeably.

We distinguish between the fundamental components of the currents and fluxes, which we denote by the subscript 1, and their harmonics, which are indicated by the subscript hh. By integrating (2) and neglecting all resistances, we obtain the fundamental-component system model

$$\frac{\sqrt{3}}{3} D\Psi_{1,\alpha\beta} = L_{\mathrm{eq}} i_{1,\alpha\beta} + \Psi_{\mathrm{PCC},\alpha\beta}, \tag{7a}$$

$$\Psi_{1,\gamma} = L_{\mathrm{br}} i_{1,\mathrm{circ}} \tag{7b}$$

and the harmonic model

$$\Psi_{\mathrm{hh},\alpha\beta} = (L_{\mathrm{eq}} + L_{\mathrm{g}}) i_{\mathrm{hh},\alpha\beta}, \tag{8a}$$

$$\Psi_{\mathrm{hh},\gamma} = L_{\mathrm{br}} i_{\mathrm{hh,circ}}. \tag{8b}$$

In (7a), $\Psi_{\mathrm{PCC},\alpha\beta} = L_{\mathrm{g}} i_{\mathrm{g},\alpha\beta} + \Psi_{\mathrm{g},\alpha\beta}$ is the fundamental component of the virtual PCC flux, which can be estimated. The load current is considered a disturbance in (8a) and is thus neglected; its compensation is addressed by the current references from the outer control loops.

C. Reference Generation for MP^{3}C

Three computational entities provide the necessary references and inputs for MP^{3}C. These entities are shown on the left-hand side of Fig. 4.

Steady-state switching function. Given the differential-mode current reference $i^*_{\alpha\beta}$ and the estimated PCC voltage $v_{\mathrm{PCC},\alpha\beta}$, the amplitudes $|u_{123}|^*$ and relative phase angles $\angle u^*_{123}$ of the switching functions are computed. This is done for the three converter branches using the model (7). Based on the outputs of this block, an appropriate OPP is loaded and the optimal flux trajectory is defined. As such, this block relates to the steady-state rather than the transient behaviour.

During (balanced or unbalanced) steady-state operation, the amplitudes $|u_{123}|^*$ and relative phase angles $\angle u^*_{123}$ are constant. In balanced conditions, the switching functions in the three branches have the same amplitude and a relative phase shift of $\frac{2\pi}{3}$. In unbalanced conditions, however, the amplitudes of the switching functions in the three branches generally differ, as do the phase shifts between them. Such a scenario will be considered in Sect. V-C.

Flux reference phase angle. The current reference $i^*_{\alpha\beta}$ is translated into the flux reference $\Psi^*_{\alpha\beta}$ with (7a), and the phase angle of the flux reference $\Psi^*_{\alpha\beta}$ is computed according to $\theta^* = \arctan \Psi^*_\beta / \Psi^*_\alpha$. The latter determines the phase angle of the OPP and the corresponding optimal virtual flux reference.

Higher-order harmonic flux reference. $\Psi^*_{\mathrm{hh},\alpha\beta\gamma}$ is derived from the harmonic references $i^*_{\mathrm{hh},\alpha\beta}$ and $i^*_{\mathrm{hh,circ}}$ using (8).

D. Multilevel MP^{3}C

MP^{3}C tracks the flux references while preserving the optimal harmonic spectrum of the OPP. Its block diagram is shown in Fig. 5 and described hereafter.

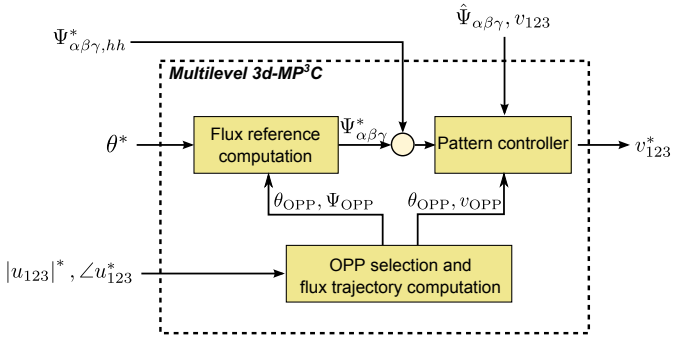

Fig. 5: Block diagram of multilevel MP^{3}C

OPP selection and flux trajectory. Based on the required fundamental component of the switching function, the OPPs are loaded from the memory. First, starting from the primary switching angles and switching sequence, the switching pattern over the fundamental period is unwrapped by exploiting quarter-wave symmetry. Second, the virtual flux trajectory corresponding to the OPPs is computed. To do so, the switching function is multiplied by the nominal module capacitor voltage to obtain the nominal branch voltage. This voltage is then integrated over time to obtain the virtual flux trajectory. Any dc component is removed. Since the nominal branch voltage is piecewise constant, the resulting virtual flux trajectory is piecewise affine. It thus suffices to compute its corner points, in between which the trajectory can be interpolated.

Note that for unbalanced operating conditions, three different OPPs are usually required for the three converter branches. These OPPs have different fundamental components with different amplitudes and phase shifts between them. It is therefore advisable to compute the corner points of the virtual flux trajectory online (rather than offline).

Moreover, note that unlike for classical OPP-based control systems, dynamic control is not accomplished by switching to a new OPP, but rather by modifying the OPP through MP^{3}C. The virtual flux trajectory based on the OPP is optimal in the sense that it "encodes" the optimal harmonic current spectrum that meets the grid codes. By tracking this virtual flux trajectory, we ensure that during steady-state operation the optimal harmonic spectrum is obtained despite variations in the capacitor voltages of the modules, system delays and small disturbances.

Flux reference vector. The flux reference angle θ^* determines the point on the virtual flux reference trajectory that is to be tracked. The exact point on the reference trajectory is obtained by interpolating between its corner points using $\theta_{\mathrm{OPP},i}$ and $\Psi_{\mathrm{OPP},\alpha\beta\gamma,i}$.

Pattern controller. The predictive pattern controller is based on the following principle: A flux error in the jth branch $\Delta\Psi_j = \Psi^*_j - \Psi_j$ can be removed by shifting the upcoming OPP switching transitions by the time $\Delta t_j = -\frac{\Delta\Psi_j}{\Delta u_j v_\mathrm{c}}$, where Δu_j is the sign of the upcoming switching transition and v_c is the nominal capacitor voltage. Positive Δt_j imply that the switching transition needs to be postponed, whereas negative Δt_j mean that the switching transition needs to be moved to an earlier moment. This simple observation follows directly from the definition of the virtual flux (6) and the assumption of the branch voltages being piecewise constant waveforms.

In the stationary orthogonal reference frame, the flux error compensation problem can be formulated as the constrained optimization problem

$$\min_{\Delta t} \left\| \Psi^*_{\alpha\beta\gamma} - \hat{\Psi}_{\alpha\beta\gamma} - \Psi_{\alpha\beta\gamma,\mathrm{corr}}(\Delta t) \right\|_2^2 + \Delta t^T Q \Delta t \quad \text{(9a)}$$

$$\text{subj. to } kT_s \le t_{11} \le t_{12} \le \cdots \le t_{1n_1} \le t^*_{1(n_1+1)} \quad \text{(9b)}$$

$$kT_s \le t_{21} \le t_{22} \le \cdots \le t_{2n_2} \le t^*_{2(n_2+1)} \quad \text{(9c)}$$

$$kT_s \le t_{31} \le t_{32} \le \cdots \le t_{3n_3} \le t^*_{3(n_3+1)}. \quad \text{(9d)}$$

The number of OPP switching transitions in the prediction horizon is denoted by n_1, n_2 and n_3 for the three branches. The ith nominal switching instant and the ith switching transition in branch 1 are denoted by t^*_{1i} and Δu^*_{1i}, respectively, and analogously for the branches 2 and 3.

The corrections of the switching instants are aggregated in the optimization variable $\Delta t = [\Delta t_{11} \quad \Delta t_{12} \ldots \Delta t_{1n_1} \quad \Delta t_{21} \ldots \Delta t_{2n_2} \quad \Delta t_{31} \ldots \Delta t_{3n_3}]^T$. For branch 1, for example, the correction of the ith switching instant is given by $\Delta t_{1i} = t_{1i} - t^*_{1i}$, where t_{1i} denotes the modified ith switching instant.

The flux error is given by $\Psi^*_{\alpha\beta\gamma} - \hat{\Psi}_{\alpha\beta\gamma}$, where $\hat{\Psi}_{\alpha\beta\gamma}$ is the flux estimate. The correction of the flux throughout the prediction horizon is given by

$$\Psi_{\alpha\beta\gamma,\mathrm{corr}}(\Delta t) = -M_{\alpha\beta\gamma} v_\mathrm{c} \cdot \left[\sum_{i=1}^{n_1} \Delta t_{1i} \Delta u_{1i} \quad \sum_{i=1}^{n_2} \Delta t_{2i} \Delta u_{2i} \quad \sum_{i=1}^{n_3} \Delta t_{3i} \Delta u_{3i} \right]^\mathrm{T}.$$

Note that the flux correction is a linear function in the optimization variable. Its squared two norm, denoted by $||\cdot||_2^2$, is then a quadratic function in Δt. The term $\Delta t^T Q \Delta t$ in the objective function (9a) penalizes modifications of the switching instants with the aim to preserve the nominal OPP if possible. It is also a quadratic function of Δt.

The constraints (9b)–(9d) ensure that the order of the switching transitions is kept in each branch. That means that each switching transition can be moved forward in time at most until the previous switching instant in the same branch or, in the case of the first upcoming switching instant, to the current time step kT_s. The switching transition can be delayed at most until the next switching transition in the same branch or, in the case of the last switching transition considered in the optimization, until the next OPP switching instant that is scheduled beyond the prediction horizon.

These constraints are linear and the objective function is quadratic in the optimization variable. This implies that the optimization problem (9) underlying MP^{3}C is a quadratic program (QP). Highly efficient solvers are readily available to solve such QPs.

We design a model predictive controller (MPC) based on the receding horizon control principle. The controller solves the optimization problem (9) at each sampling instant kT_s and

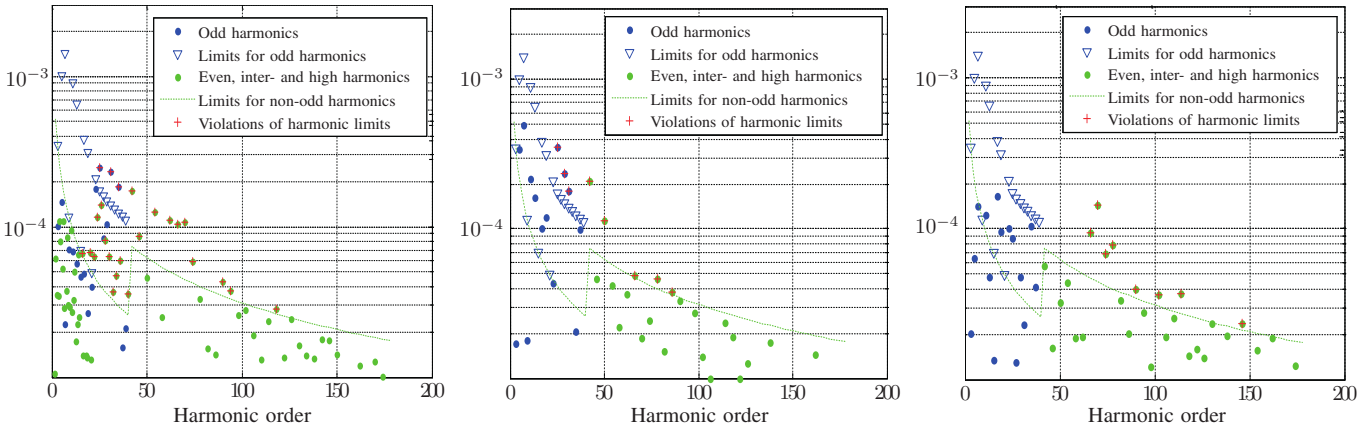

(a) Carrier-based PWM with 100% switching losses (b) MP^{3}C with the switching losses reduced to 41% (c) MP^{3}C with 101% switching losses

Fig. 6: Steady-state operation at nominal capacitive reactive power: harmonic current spectrum

computes the average voltage level reference for the MMC, $v^*_{123} \in \{-M, ..., 0, ..., M\}^3$, within the sampling interval. At the next sampling instant, the new flux reference and flux estimate are obtained, and new nominal switching instants and corresponding switching transitions are read in. The optimization is repeated with the new data over a shifted prediction horizon. This controller design enables very fast reactions to disturbances and reference changes.

E. Cell Selection

The cell selection algorithm translates the voltage level reference for each converter branch to module voltage references, i.e. it decides on the modules to be inserted or removed to accomplish any required change in the voltage level. The main objective is to balance the capacitor voltages of the modules within each branch. To achieve this, the modules are sorted according to their capacitor voltages. If current flows into (out of) the branch, the module with the lowest (highest) voltage is inserted. In contrast, the module with the lowest (highest) voltage is removed, when the current flows out of (into) the branch.

V. Performance Evaluation

Consider the STATCOM in Fig. 1 with $M = 9$ modules per branch. The rated converter voltage is 10.3 kV and the rated current is in the kiloampere range. A per unit (pu) system is established based on the peak values of the rated phase voltage and current. The inductors are $L_{\text{br}} = L_{\text{sc}} = L_{\text{g}} = 0.1\,\text{pu}$ and the resistors are $R_{\text{br}} = R_{\text{sc}} = R_{\text{g}} = 0.005\,\text{pu}$. The sampling interval of the controller is $25\mu s$.

A. Steady-State Operation

The harmonic spectra of the STATCOM output current are depicted in Fig. 6. All harmonics around a given integer harmonic, including inter-harmonics, are grouped to this integer harmonic by computing the RMS value of their amplitudes. The amplitude of the resulting harmonic is then normalized using the short-circuit current, and the harmonic spectra are compared with the grid code. The operating point is at nominal capacitive power ($Q = 1\,\text{pu}$) injected into the grid.

Three different control scenarios are considered hereafter. Fig. 6(a) depicts the current spectra for asynchronous carrier-based PWM (CB-PWM). We use this standard modulation method to provide a baseline in terms of harmonic performance and switching losses. The harmonic current spectrum in Fig. 6(b) results from the proposed MP^{3}C method. The switching frequency is approximately 2.5 times lower than for CB-PWM. As a result, the switching losses are reduced by approximately the same factor, whereas the harmonic spectrum is similar to that of CB-PWM. Lower switching losses increase the system efficiency, allow for a cheaper cooling system, and extend the lifetime of the semiconductor switches.

Alternatively, MP^{3}C may use the same switching frequency, and correspondingly approximately the same switching losses, as CB-PWM. The harmonic spectrum is, however, superior, as shown in Fig. 6(c). The grid codes are met up to the 66th harmonic, whereas for CB-PWM, the first violation occurs already at the 16th harmonic. We conclude that MP^{3}C enables a significant reduction of an output filter.

It is interesting to notice that the harmonic spectra are qualitatively quite different—MP^{3}C produces little even and inter-harmonics, which are penalized more heavily by the grid code. The odd harmonics in the lower end of the spectrum meet the grid code, but are not fully eliminated. This shaping of the OPP's harmonic spectrum extends the frequency range over which the grid code can be met.

B. Reactive Power Reference Step

The dynamic response to a reactive power reference step is simulated next. An extreme transient from nominal inductive power $Q = -1\,\text{pu}$ to nominal capacitive power $Q = 1\,\text{pu}$ is considered. The active and reactive power are shown in Fig. 7(a). The latter exhibits a very fast response, with the power transient lasting for less then 5 ms, i.e. less than a quarter of the fundamental period. During this transient, the phase of the current is shifted by 180°, as can be seen in Fig. 7(b).

The branch voltages are depicted in Fig. 7(c). Before and after the transient, the characteristic switching pattern of the

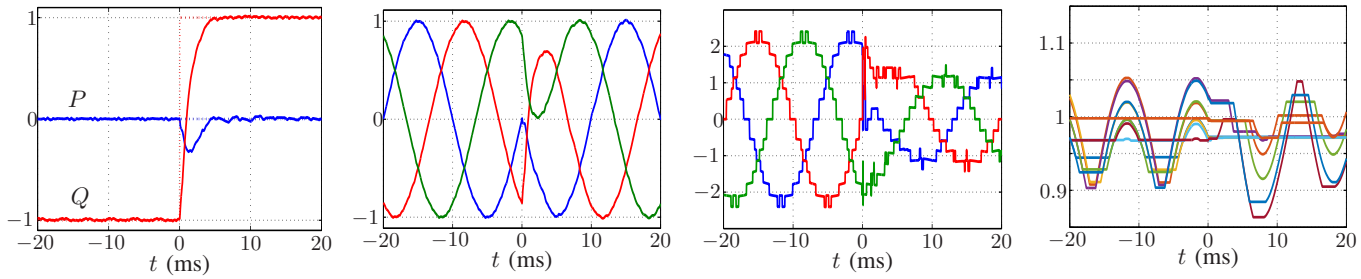

(a) Active power P (pu) and reactive power Q (pu)

(b) Phase currents i_{abc} (pu)

(c) Branch voltages v_{123} (pu)

(d) Capacitor voltages v_{c1i} (pu) of the 9 modules in branch 1

Fig. 7: Reactive power reference step from -1 to 1 pu at time $t = 0$. The power references are shown as dotted lines

OPP is clearly recognizable. During the transient, however, MP^{3}C strongly modifies the pulse pattern in order to accomplish a fast transient. To facilitate this, pulse insertion as described in [11] is used for the MP^{3}C algorithm. The capacitor voltages of the individual modules are disturbed by the transient. The dc components of the capacitor voltages are offset by at most 25% of their peak-to-peak voltage ripple. The cell selection algorithm quickly removes any dc offset and restores the equilibrium within two fundamental periods. This is exemplified in Fig. 7(d) for the first branch.

C. Negative-Sequence Current Injection

Consider the balanced grid voltage

$$v_{g,a} = \sin(\omega t),\ v_{g,b} = \sin(\omega t - \frac{2\pi}{3}),\ v_{g,c} = \sin(\omega t + \frac{2\pi}{3})$$

and unbalanced operation, in which the STATCOM is required to inject a negative-sequence current with the reference

$$i^*_{g,a} = \sin(\omega t),\ i^*_{g,b} = \sin(\omega t + \frac{2\pi}{3}),\ i^*_{g,c} = \sin(\omega t - \frac{2\pi}{3})$$

into the grid. To accomplish this, the fundamental component of the virtual branch flux is required to be

$$\Psi_{1,\alpha\beta} = \sqrt{3} D^T \begin{bmatrix} (\Psi_{\mathrm{PCC},\alpha\beta} + L_{\mathrm{eq}} i_{1,\alpha\beta}) \cos(\omega t) \\ (\Psi_{\mathrm{PCC},\alpha\beta} - L_{\mathrm{eq}} i_{1,\alpha\beta}) \sin(\omega t) \end{bmatrix}$$

according to (7a).

The two components in stationary coordinates have different amplitudes, implying different amplitudes for the branch voltages, which is typical for operation under unbalanced conditions. The trajectories of the grid flux, converter flux and the injected current in stationary coordinates are shown in Fig. 8. Note that the current phasor rotates in the opposite direction from the grid and converter flux phasors.

The corresponding simulation results are summarized in Fig. 9. Figs. 9(a) and 9(b) show that the grid voltages and the injected currents have the expected phase shifts. Phases a, c and b of the three-phase current are aligned with phases a, b and c of the grid voltage. Fig. 9(c) shows the branch voltages, which have, as expected, different amplitudes and use different OPPs. Accordingly, the currents in the three branches differ significantly, with branch 2 exhibiting a low current amplitude, as can be seen in Fig. 9(d).

This implies a significant circulating current in the converter, as shown in Fig. 9(e). The reference for the circulating

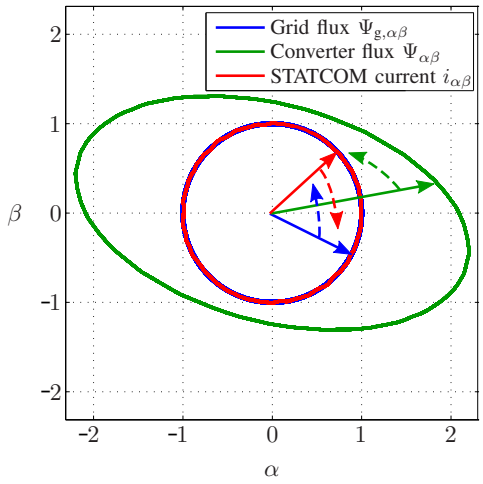

Fig. 8: Injection of a negative-sequence current: virtual flux and current trajectories in stationary coordinates

current is determined from the flux reference Ψ^*_γ according to (7b). The latter is obtained by combining three different OPP voltages, integrating the voltages to obtain flux trajectories, converting the trajectories to stationary coordinates and removing the dc offset. The tracking of Ψ^*_γ is accomplished by MP^{3}C.

D. Harmonic Current Injection

Last, the system response to the asymmetrical harmonic current reference

$$\begin{aligned} i^*_{\mathrm{hh},a} &= 0.04\big(\sin(3\omega t) + \sin(11\omega t)\big), \\ i^*_{\mathrm{hh},b} &= -0.04\big(\sin(3\omega t) + \sin(11\omega t)\big), \\ i^*_{\mathrm{hh},c} &= 0 \end{aligned}$$

is investigated. The current tracking in the time domain is shown in Fig. 10(a), whereas Fig. 10(b) depicts the harmonic spectrum of the three-phase output current. The tracking performance is good, particularly in light of the low device switching frequency of 150 Hz. The inserted 4th and 11th harmonics can be clearly identified in the harmonic spectrum.

To track these references, the control system purely relies on the corrections to the switching instants done by MP^{3}C. The latter uses the pulse insertion mechanism described in [11] to improve the tracking performance.

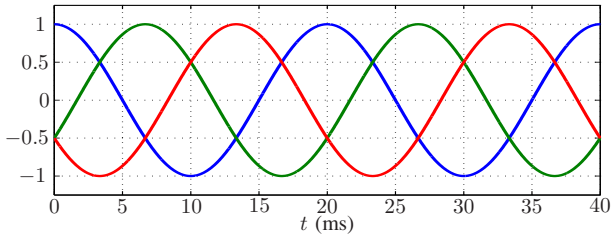

(a) Grid voltage v_{abc} (pu)

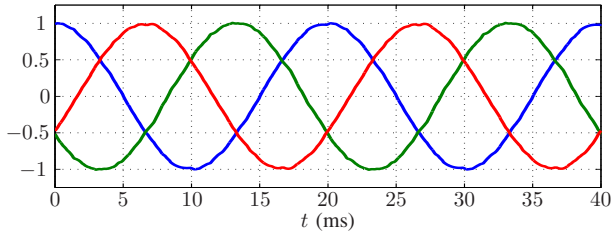

(b) Grid current i_{abc} (pu)

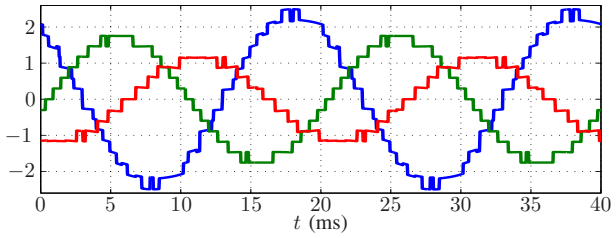

(c) Branch voltage v_{123} (pu)

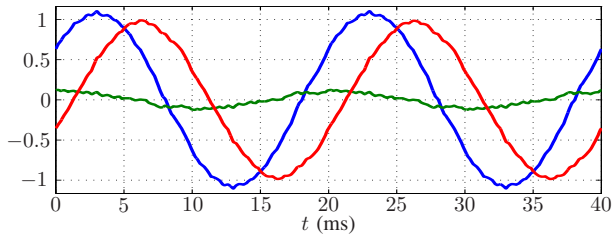

(d) Branch current i_{123} (pu)

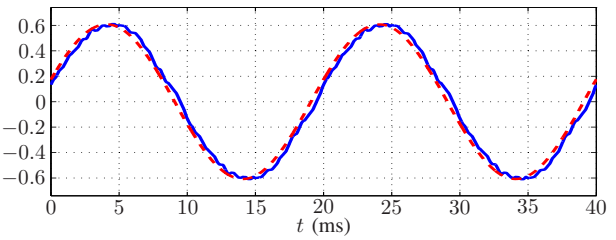

(e) Circulating current i_{circ} (pu)

Fig. 9: Injection of a negative-sequence current

VI. Conclusion

An OPP-based control system for delta-connected MMC STATCOMs was proposed in this paper. By computing OPPs that meet the relevant grid codes, the MP^{3}C scheme provides an excellent harmonic current spectrum while operating at device switching frequencies below 200 Hz. Compared to classical control and modulation methods, (i) the switching losses can be either reduced for a similar current spectrum, or (ii) the current spectrum can be significantly improved for similar switching losses.

This increases the system efficiency and reduces the size of the output filter, lowering the cost of the overall converter system. Thanks to the fast MPC-based control methodology modifying the OPPs, the proposed control scheme is able to address the control objectives inherent to STATCOMs, such as very fast system responses, operation under imbalances and compensation of harmonics at the PCC.

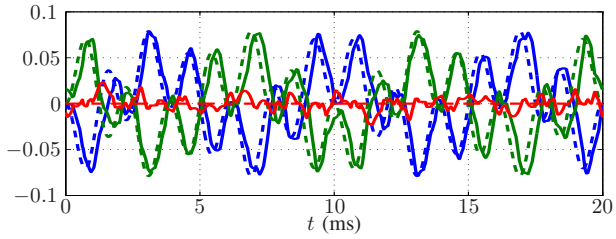

(a) Tracking of the output current reference i^*_{abc} (pu). Dashed lines are the references and the solid lines are the measured phase currents

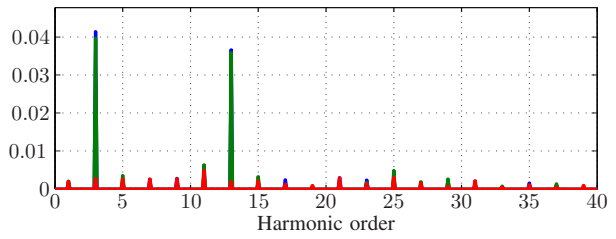

(b) Amplitudes of the harmonic spectrum of i_{abc} (pu)

Fig. 10: Injection of a harmonic output current. The colours blue, green and red refer to phase a, b and c, respectively

References

[1] Bundesverband der Energie- und Wasserwirtschaft e.V. (BDEW), "Erzeugungsanlagen am Mittelspannungsnetz. Richtlinie für Anschluss und Parallelbetrieb von Erzeugungsanlagen am Mittelspannungsnetz," Jun. 2008.

[2] A. Lesnicar and R. Marquardt, "An innovative modular multilevel converter topology suitable for a wide power range," in *Proc. IEEE Power Tech. Conf.*, (Bologna, Italy), Jun. 2003.

[3] H. M. Pirouz and M. T. Bina, "Modular multilevel converter based STATCOM topology suitable for medium-voltage unbalanced systems," *J. of Power Electron.*, vol. 10, pp. 572–578, Sep. 2010.

[4] I. Colak, E. Kabalci, and R. Bayindir, "Review of multilevel voltage source inverter topologies and control schemes," *Energy Convers. and Mgmt.*, vol. 52, pp. 1114–1128, Feb. 2011.

[5] J. E. Huber and A. J. Korn, "Optimized pulse pattern modulation for modular multilevel converter high-speed drive," in *Proc. Int. Power Electron. and Motion Control Conf.*, (Novi Sad, Serbia), Sep. 2012.

[6] T. Geyer, N. Oikonomou, G. Papafotiou, and F. Kieferndorf, "Model predictive pulse pattern control," *IEEE Trans. Ind. Appl.*, vol. 48, pp. 663–676, Mar./Apr. 2012.

[7] H. Patel and R. Hoft, "Generalized techniques of harmonic elimination and voltage control in thyristor inverters: Part I–Harmonic elimination," *IEEE Trans. Ind. Appl.*, vol. IA-9, pp. 310–317, May/Jun. 1973.

[8] H. Akagi, "New trends in medium-voltage power converters and motor drives," in *Proc. IEEE Int. Symp. Ind. Electron.*, Jun. 2011.

[9] T. Geyer, *Model predictive control of high power converters and industrial drives*. London, UK: Wiley, Oct. 2016.

[10] R. Picas, J. Pou, S. Ceballos, J. Zaragoza, G. Konstantinou, and V. Angelidis, "Optimal injection of harmonics in circulating currents of modular multilevel converters for capacitor voltage ripple minimization," in *ECCE Asia Downunder*, pp. 318–324, Jun. 2013.

[11] T. Geyer and N. Oikonomou, "Model predictive pulse pattern control with very fast transient responses," in *Proc. IEEE Energy Convers. Congr. Expo.*, (Pittsburgh, PA, USA), Sep. 2014.